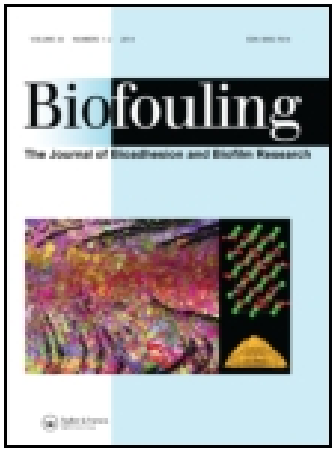

Biofouling: The Journal of Bioadhesion and Biofilm Research

Publication details, including instructions for authors and subscription information:
http://www.tandfonline.com/loi/gbif20

Alumina surfaces with nanoscale topography reduce attachment and biofilm formation by Escherichia coli and Listeria spp.

Guoping Feng[a], Yifan Cheng[a], Shu-Yi Wang[b], Lillian C. Hsu[a], Yazmin Feliz[b], Diana A. Borca-Tasciuc[b], Randy W. Worobo[a] & Carmen I. Moraru[a]

[a] Department of Food Science, Cornell University, Ithaca, NY, USA

[b] Department of Mechanical, Aerospace and Nuclear Engineering, Rensselaer Polytechnic Institute, Troy, NY, USA

Published online: 27 Nov 2014.

Biofouling, 2014
Vol. 30, No. 10, 1253–1268, http://dx.doi.org/10.1080/08927014.2014.976561

Taylor & Francis
Taylor & Francis Group

Alumina surfaces with nanoscale topography reduce attachment and biofilm formation by *Escherichia coli* and *Listeria* spp.

Guoping Feng[a], Yifan Cheng[a], Shu-Yi Wang[b], Lillian C. Hsu[a], Yazmin Feliz[b], Diana A. Borca-Tasciuc[b]*, Randy W. Worobo[a] and Carmen I. Moraru[a]*

[a]*Department of Food Science, Cornell University, Ithaca, NY, USA;* [b]*Department of Mechanical, Aerospace and Nuclear Engineering, Rensselaer Polytechnic Institute, Troy, NY, USA*

(*Received 16 May 2014; accepted 8 October 2014*)

This work reports on a simple, robust and scientifically sound method to develop surfaces able to reduce microbial attachment and biofilm development, with possible applications in medicine, dentistry, food processing, or water treatment. Anodic surfaces with cylindrical nanopores 15 to 100 nm in diameter were manufactured and incubated with *Escherichia coli* ATCC 25922 and *Listeria innocua*. Surfaces with 15 and 25 nm pore diameters significantly repressed attachment and biofilm formation. Surface–bacteria interaction forces calculated using the extended Derjaguin Landau Verwey-Overbeek (XDLVO) theory indicate that reduction in attachment and biofilm formation is due to a synergy between electrostatic repulsion and surface effective free energy. An attachment study using *E. coli* K12 strains unable to express appendages also suggests that the small-pore surfaces may inhibit flagella-dependent attachment. These results can have immediate, far-reaching implications and commercial applications, with substantial benefits for human health and life.

Keywords: nanoscale anodized alumina; bacterial attachment; biofilms; *Escherichia coli*; *Listeria*

Introduction

Biofilm formation by pathogenic bacteria has harmful, sometimes fatal, consequences and can pose severe contamination problems in medicine, dentistry, food processing, and water treatment. Colonization by bacteria on medical devices and biofilm-related infections account for 80% of all human bacterial infections (Taylor et al. 2012). Nosocomial infections in hospital settings, commonly associated with contaminated medical devices, represent one of the leading causes of death in the USA (Bryers 2009). Biofilms formed by pathogenic organisms in food processing plants are a major culprit in foodborne diseases, which claim thousands of lives and amount to losses of about $78 billion/year in the USA alone (Scharff 2012). Therefore, significant efforts are made to develop solutions for preventing biofilm formation and microbial contamination in environments that directly affect human health and life.

Bacterial attachment is the first step in the development of biofilms, which are cohesively structured matrices, notoriously difficult to remove by physical and chemical means. Besides microbial cell surface properties and environmental factors, the physico-chemical properties of the surface, including topography and roughness, free surface energy and surface charge are critical to bacteria attachment and biofilm formation (Rijnaarts et al. 1999; Oliveira et al. 2001; Verran & Boyd 2001; Mauclaire et al. 2010; Singh et al. 2011).

The effects of surface topography and roughness at the micrometer scale on attachment have been extensively studied, sometimes with contradictory findings. Several studies conducted with microorganisms of interest for medicine and food processing, including *Streptococcus thermophilus*, *Streptococcus waiu*, *Listeria monocytogenes*, and *Flavobacterium odoratum*, reported inconclusive correlations between surface roughness and bacterial adhesion (Boulangé-Petermann et al. 1997; Tide et al. 1999; Verran & Boyd 2001). In contrast, other studies indicated a significant impact of surface roughness on attachment (Arnold & Bailey 2000; Medilanski et al. 2002). A defined surface topography has also been shown to influence bacterial attachment. Surfaces with channels, pits or pillars of dimensions comparable to bacterial cells appear to impact bacterial attachment, while surface details at a scale larger than the cell size do not affect it significantly (Whitehead et al. 2005; Díaz et al. 2007; Verran et al. 2010; Xu & Siedlecki 2012). Some of these effects are in part due to the interaction between the bacterial adhesins including flagella, fimbriae, or curli, with elements of surface topography (Prigent-Combaret et al. 2000; Lemon et al. 2007; Niba et al. 2007). A study by Friedlander et al. (2013)

*Corresponding authors. Email: borcad@rpi.edu (D.A. Borca-Tasciuc); cim24@cornell.edu (C.I. Moraru)

reported that flagella expressed by *E. coli* can reach into surface crevices and act as structural elements in attachment and biofilm formation. Work from the authors' group also indicates significant differences in expression of cellular appendages as a response to surface topography in the micro- and nanoscale range (Hsu et al. 2013).

Attachment of bacteria to nanostructured surfaces is significantly different from attachment on bulk or microstructured materials (Park et al. 2008; Puckett et al. 2010). Explanations of this behavior allude to the fact that nanostructuring induces significant changes in surface charge and surface free energy, which affect attachment and biofilm formation (Hori & Matsumoto 2010). There is therefore a great opportunity to design nanostructured materials able to effectively repel microorganisms. Unfortunately, most nanostructuring methods are expensive, which renders the approach prohibitively expensive for many applications. Nanostructured surfaces can also be extremely delicate and incompatible with the cleaning procedures used in industrial or medical applications.

Compared to other nanofabrication methods, anodization is a widely available surface treatment that produces an oxide which, under well controlled conditions, exhibits a nanoporous structure, is chemically inert to many cleaning agents, and has excellent wearing properties. Anodization is used on an industrial scale and can be applied to large surface areas and three-dimensional parts. Aluminum anodization in particular is a widely used process, with countless industrial applications (Thomas & Benaben 2007). By controlling the anodizing voltage and bath composition, Al anodization produces cylindrical, parallel pores oriented perpendicular to the surface, of defined pore diameter and surface porosity (Jessensky et al. 1998; Masuda et al. 1998).

This study explores the effect of nanoscale topography created by anodization on the attachment and biofilm formation by Gram-positive and Gram-negative bacteria, the mechanisms responsible for the impact of nanoscale surfaces on attachment, and demonstrates a simple yet robust solution to prevent bacterial attachment by controlling surface properties.

Materials and methods

Surface fabrication

Nanoporous aluminum oxide surfaces with pore diameters of 15, 25, 50 and 100 nm were prepared by two-step anodization of high purity aluminum (99.99%, Alfa Aesar, Ward Hill, MA, USA). The Al substratum was first subjected to mechanical and electrochemical polishing. An annealing process was performed between the two polishing steps to release internal stresses (Jessensky et al. 1998). The Al substratum was then immersed in an etchant to remove the thin alumina layer formed during electrochemical polishing. The first anodization step was then carried out using a setup similar to that used for electrochemical polishing, but the reaction was carried out at room temperature. The voltage and anodizing mixture depended on the pore size. The first porous alumina layer was etched away and a second anodization step was performed, during which pore growth was initiated from dents left over by the nanopores in the first layer, resulting in regular surface features (Jessensky et al. 1998; Masuda et al. 1998). Nanosmooth aluminum oxide surfaces of 10 × 10 × 0.5 mm (Alfa Aesar) were used as a control. It is also important to note that Al oxide (alumina) is a generally recognized as safe (GRAS) material.

Bacterial cultures and media

The bacterial strains used were the Gram-negative *E. coli* ATCC 25922, which has been used as a surrogate for *E. coli* O157:H7 in attachment studies (Kim & Harrison 2009), and the Gram-positive *L. innocua* FSL C2-008; *L. innocua* has been used in previous attachment studies as surrogates for pathogenic *L. monocytogenes* (Saini et al. 2012). Four strains of *E. coli* K12: wild type (WT), flagellum-deficient (*ΔflgA*), fimbriae-deficient (*ΔfimH*) and curli-deficient (*ΔcsgA*) mutants were used to study the impact of surface adhesins on attachment. The *E. coli* K12 strains were obtained from the National BioResource Project at National Institute of Genetics (Mishima, Shizuoka, Japan). All cultures were maintained at –80°C in tryptic soy broth (TSB) (Difco, Becton Dickinson and Company, Sparks, MD, USA) with 20% (v/v) glycerol. *E. coli* K12 mutant strains were maintained in the same medium, with 30 μg ml^{-1} of kanamycin. The strains were reactivated on tryptic soy agar (TSA, Difco), then grown in capped culture tubes with TSB at 37°C, with shaking at 225 rpm.

Characterization of surfaces by scanning electron microscopy (SEM)

The surface topographic features and bacterial attachment were visualized using a Zeiss LEO 1550 field emission SEM (Carl Zeiss Microscopy, Jena, Germany). For analyzing the bare surfaces, coupons of each substratum were cleaned using two cycles of 30-min sonication in Milli-Q water, then rinsing in absolute ethanol. For visualizing surfaces with attached bacteria, surfaces were retrieved after incubation for 48 h and rinsed in sterile water to remove unattached cells. Bacteria attached to surfaces were fixed using 2.5% (w/v) glutaraldehyde in 0.05 M sodium cacodylate buffer at 4°C for 2 h. Samples were rinsed in cacodylate buffer three times, 5 min each time, then subjected to a secondary fixation using 1% (w/v) osmium tetroxide in cacodylate buffer, for 1 h. The fixed samples were rinsed in cacodylate buffer three times, then dehydrated using ethanol solutions of 25%

(v/v), 50%, 70%, 95%, 100% and 100% for 10 min each, followed by critical point-drying with carbon dioxide. Dried surfaces were mounted to SEM stubs and coated with evaporated carbon. A voltage of 1–5 kV was used, depending on the sample. Images were acquired using the SmartSEM software (Carl Zeiss Microscopy).

Bacterial attachment and biofilm formation

Bacterial strains were sub-cultured from freshly streaked colonies on TSA in 4 ml of TSB for 24 h. A volume of 10 µl of culture was transferred to 3 ml of fresh TSB and incubated for 12–16 h. The alumina surfaces were cleaned using two cycles of 30-min sonication in Milli-Q water, and sterilized with absolute ethanol. The sterilized surfaces were vertically placed in TSB containing the *E. coli* or *L. innocua* culture, without shaking, and incubated at 37°C for up to 96 h.

Visualization and quantification of biofilm matrices using confocal laser scanning microscopy (CLSM)

Surfaces prepared as above were sampled after incubation for 30 min, 48 h and 96 h. The surfaces were vertically placed in stationary phase *E. coli* ATCC 25922 and *L. innocua* cultures at 37°C for 30 min. TSB with a 1:100 (v/v) inoculation from 16 h old cultures was used for incubation with surfaces for the 48 and 96 h time points. The alumina surfaces with attached cells were removed gently from the culture and rinsed in sterile saline solution (0.15 M NaCl) three times, to remove unattached cells. Biofilms were labeled with Live/Dead BacLight Syto 9 and propidium iodide and rinsed with saline solution as described by Feng et al. (2013). Attached cells and biofilms were visualized using a Zeiss 710 confocal laser scanning microscope with upright objectives. Images were acquired with a Plan-Apochromat 25 × oil immersion objective lens at a scanning speed of 9 and frame pixels of 512 × 512 (surface area of 338.4 × 338.4 µm^2). The laser power and pinhole were set to 2.8% and 1.0 Airy unit, respectively. The attached cells and biofilms attached to the surface were scanned in 3D mode with a step size of 1.0 µm. Five randomly selected, evenly spaced spots per surface were chosen for scanning. Three-dimensional structures of biofilm matrices were constructed and visualized using the Volocity software (version 5.2.1, PerkinElmer, Waltham, MA, USA).

The biomass volume (µm^3 µm^{-2}) and thickness were quantified using COMSTAT (Heydorn et al. 2000), for live bacteria only. Although dead cells were observed in the biofilm, they were most likely naturally dead due to extended time of incubation, since the surfaces used in the study were not expected to have bactericidal effects.

The role of bacterial appendages in initial attachment to nanoporous alumina surfaces

E. coli K12 isogenic mutant strains of wild type (WT) and genes of *flgA*, *fimH* and *csgA* were selected from the Keio mutant library, based on previous findings that knockout of these genes resulted in significant reduction in biofilm formation (Baba et al. 2006; Niba et al. 2007). *flgA*, *fimH* and *csgA* encode major assembly protein for the flagellar basal-body periplasmic P ring, the Type 1 fimbriae adhesin unit, and the curlin major unit, respectively. Bacterial attachment was quantified by plating the cells detached from surfaces onto TSA and expressed as CFU cm^{-2}, according to a method described previously (Boulangé-Petermann et al. 1997) with minor modifications. All strains were loop-inoculated and cultured in TSB at 37°C for 16 h with aeration (225 rpm), then sub-cultured in fresh medium by a 1:100 (v./v.) inoculation until cell density reached $OD_{600\ nm}$=1.1 (10^9 cells ml^{-1}). Surfaces with 15 and 100 nm pore size were vertically placed in 3 ml of TSB containing each strain at 37°C. The surfaces were retrieved after 30 min and rinsed three times in 15 ml of 0.15 M NaCl solution to remove loosely attached cells, then sonicated in 2 ml of 0.15 M NaCl for 10 min to detach all attached cells. The recovered cell suspension was serially diluted and plated on TSA, and incubated overnight at 37°C. The experiments were repeated independently at least three times.

Measurement of contact angles

Contact angles of bacterial cell lawns and alumina substrates were determined by the sessile drop method using a Rame-Hart 500 goniometer (Rame-Hart Inc., Succasunna, NJ, USA) (Busscher et al. 1984; Li & Logan 2004). The detailed procedures are included in the Supplementary information [Supplementary information is available *via* a multimedia link on the online article webpage].

Surface charge measurements

The zeta potential of bacterial cells was measured using a Malvern Zetasizer nano-ZS with disposable folded capillary cells (Malvern Instruments, Malvern, UK). The detailed procedures are included in the Supplementary information.

Statistical analysis and mathematical modeling

Experiments were repeated independently at least three times. Each experiment included two biological samples per surface type and technical duplicates for each sample. Five random areas per surface were sampled for CLSM and data obtained from these areas was averaged to obtain a mean value for each surface. The student's *t* test was used to compare two populations. To compare

means of more than two sample populations, one-way ANOVA analysis was performed, followed by post-ANOVA Tukey's test. All statistical tests were performed using JMP 8.0 (SAS Institute, Cary, NJ, USA). The extended Derjaguin Landau Verwey-Overbeek (XDLVO) model was constructed and computed using Mathematica 9.0 (Wolfram, Champaign, IL, USA).

Results and discussion

Bacterial attachment and biofilm formation

Three dimensional images of biofilm matrices at 30 min, 48 h and 96 h obtained by CLSM are shown in Figures 1 and 2 for *E. coli* ATCC 25922 and *L. innocua* FSL C2-008, respectively. *E. coli* had an extremely low presence on the 15 and 25 nm pore surfaces, for the entire time period probed. *L. innocua* displayed the same trend, but less pronounced differences among surfaces at early stages of biofilm formation. For *E. coli*, a limited presence was also observed on the 50 nm surfaces after 30 min and 48 h; biofilm formation appeared to some extent at 96 h. On the nanosmooth control and 100 nm pore surfaces *E. coli* adhered at a significantly ($p < 0.05$) higher level than on the small pore surfaces, and a well-developed biomass was observed. The biofilm matrices formed on these two surfaces were highly structured

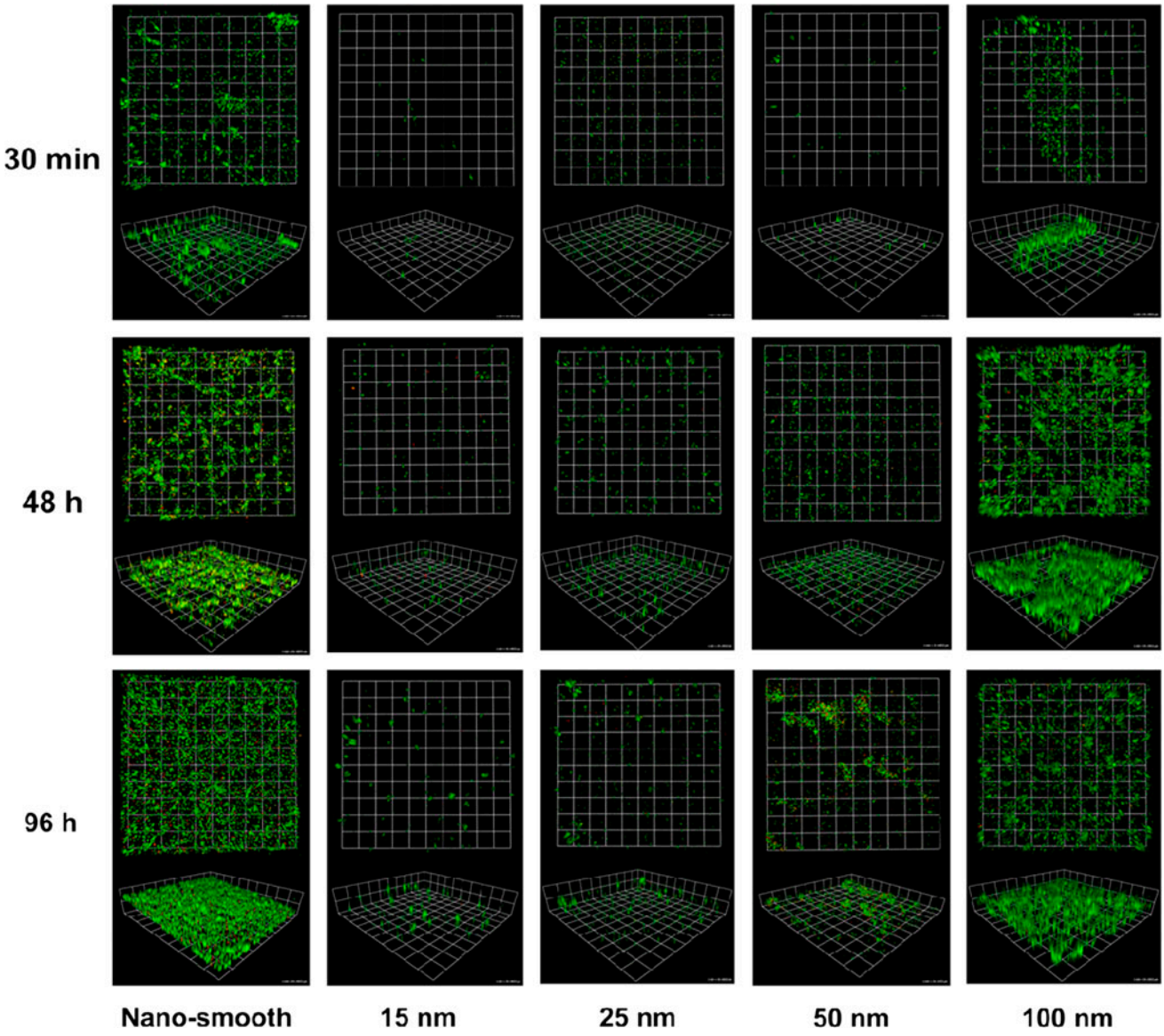

Figure 1. Constructed CLSM images of attachment and biofilm formation by live *E. coli* ATCC 25922 at 30 min, 48 h and 96 h on all alumina surfaces. These images have biomass accumulation close to the average of their surface type. Scale units (small grid) are 34 μm in length.

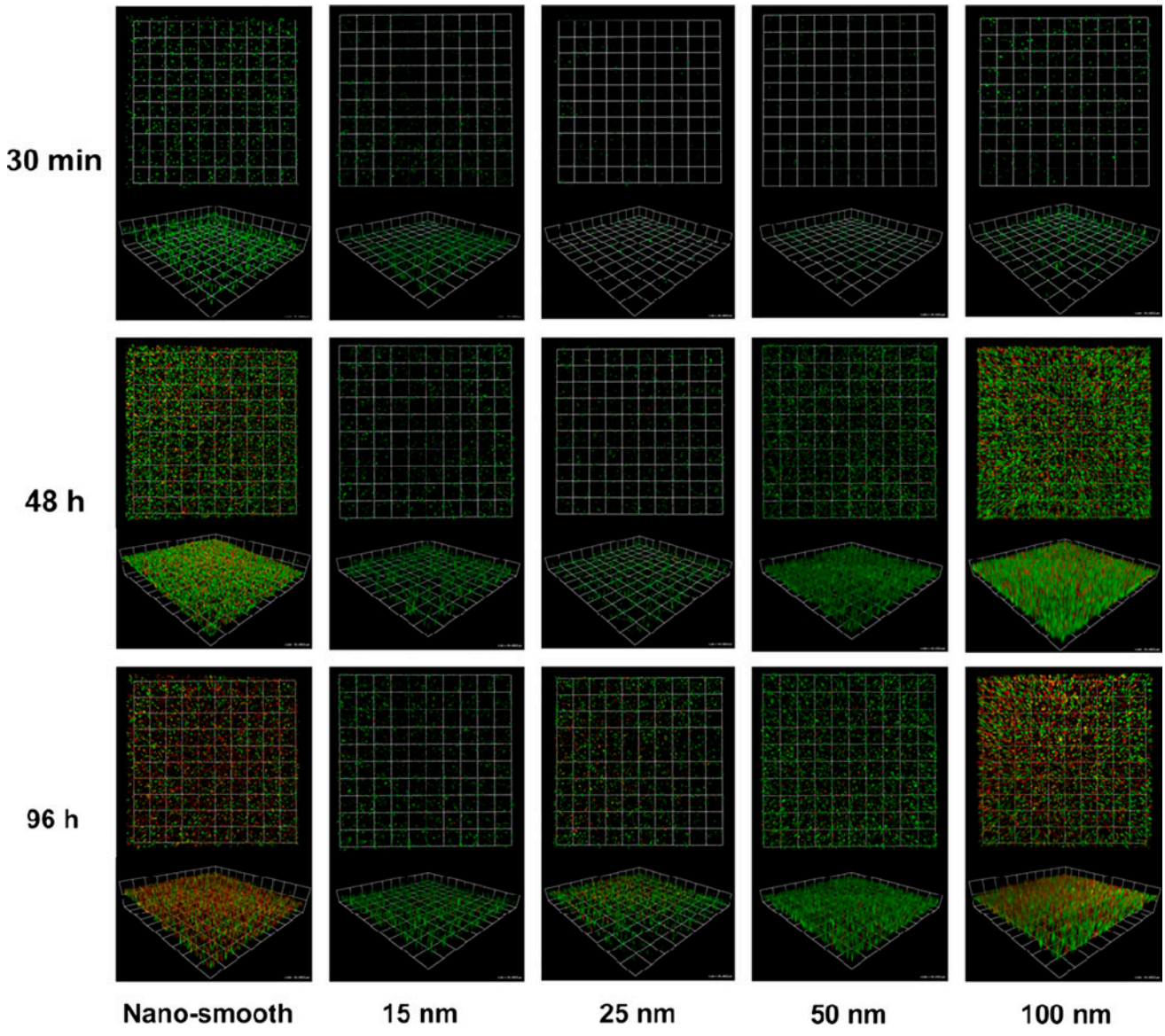

Figure 2. Constructed CLSM images of attachment and biofilm formation by live *L. innocua* at 30 min, 48 h and 96 h on all alumina surfaces. These images have biomass accumulation close to the average of their surface type. Scale units (small grid) are 34 μm in length.

laterally and vertically at 48 and 96 h, as evidenced by the volume and thickness of the biofilm layer. The 100 nm surface retained a higher amount of *E. coli* cells and a more cohesively structured biofilm than the nanosmooth surface.

A quantitative assessment of the biofilms showed that for all time points the volume of biomass formed by *E. coli* on the 15 nm surface was the least for all surfaces. At 96 h, the average biomass on this surface was 0.8 μm^3 μm^{-2}. The biomass volume for the 100 nm surface was about 15 times larger (11.8 μm^3 μm^{-2}), while for the nanosmooth control it was about 25 times larger (20.4 μm^3 μm^{-2}). At 48 h the 15 and 25 nm surfaces retained significantly less biomass than the nanosmooth control, while the biomass on the 100 nm surface was significantly higher than all the others ($p < 0.05$); the same trend was observed at 96 h.

Vertical growth often comes with a complex 3D architecture of the biofilm, which renders the biofilm more resistant to environmental stresses. In this study, thickness was used as an indicator of vertical growth of the biofilms. The average thickness of the biofilms formed by *E. coli* on all surfaces followed a trend similar as the biomass, with the 15 and 25 nm surfaces showing the smallest thickness, and the nanosmooth and 100 nm surfaces the largest thickness (Figure 3c). At 96 h the

average thickness on the 15 nm surface was 0.9 μm, which suggests the presence, on average, of a monolayer of cells. At the same time point, the thickness for the 100 nm pore size and nanosmooth control was 24.9 μm and 18.5 μm, respectively, which indicates 20 to 30 layers of cells.

L. innocua showed similar biofilm formation trends to *E. coli*, although the antifouling effects of the 15 and 25 nm pore surfaces were less pronounced (Figure 2, Figure 3b, d). At 96 h, the volume and the thickness of biomass formed by *L. innocua* on the 15 nm surface were 11.2 and 15.3 μm, respectively. On average, the 15 nm surface showed about 40% less biomass than the control and the larger pore diameter surfaces although a statistically significant difference from the control was observed only with the 25 nm surfaces (Figure 3b) at 48 h.

Overall, the CLSM observations demonstrate that anodized alumina surfaces with 15 and 25 nm pores reduced attachment and biofilm formation by *E. coli* and *L. innocua*, while the 100 nm surface promoted biofilm formation at a level similar or higher than the nanosmooth control.

A physico-chemical explanation of bacterial attachment and biofilm formation

Bacterial attachment and biofilm formation are affected by factors including the properties of the contact surface, the composition and temperature of the environment, bacterial cell physiology and cell surface properties. The interaction of bacteria cells with solid substrata has been explained before using the thermodynamic theory, which considers the surface free energy of the substratum influences both the strength and reversibility of bacterial attachment (Zhao, Liu, Wang, et al. 2005). The relationship between surface free energy and relative bacterial attachment is frequently illustrated by the 'Baier curve', which shows that the number of bacteria attached to surfaces reaches a minimum at a surface energy of

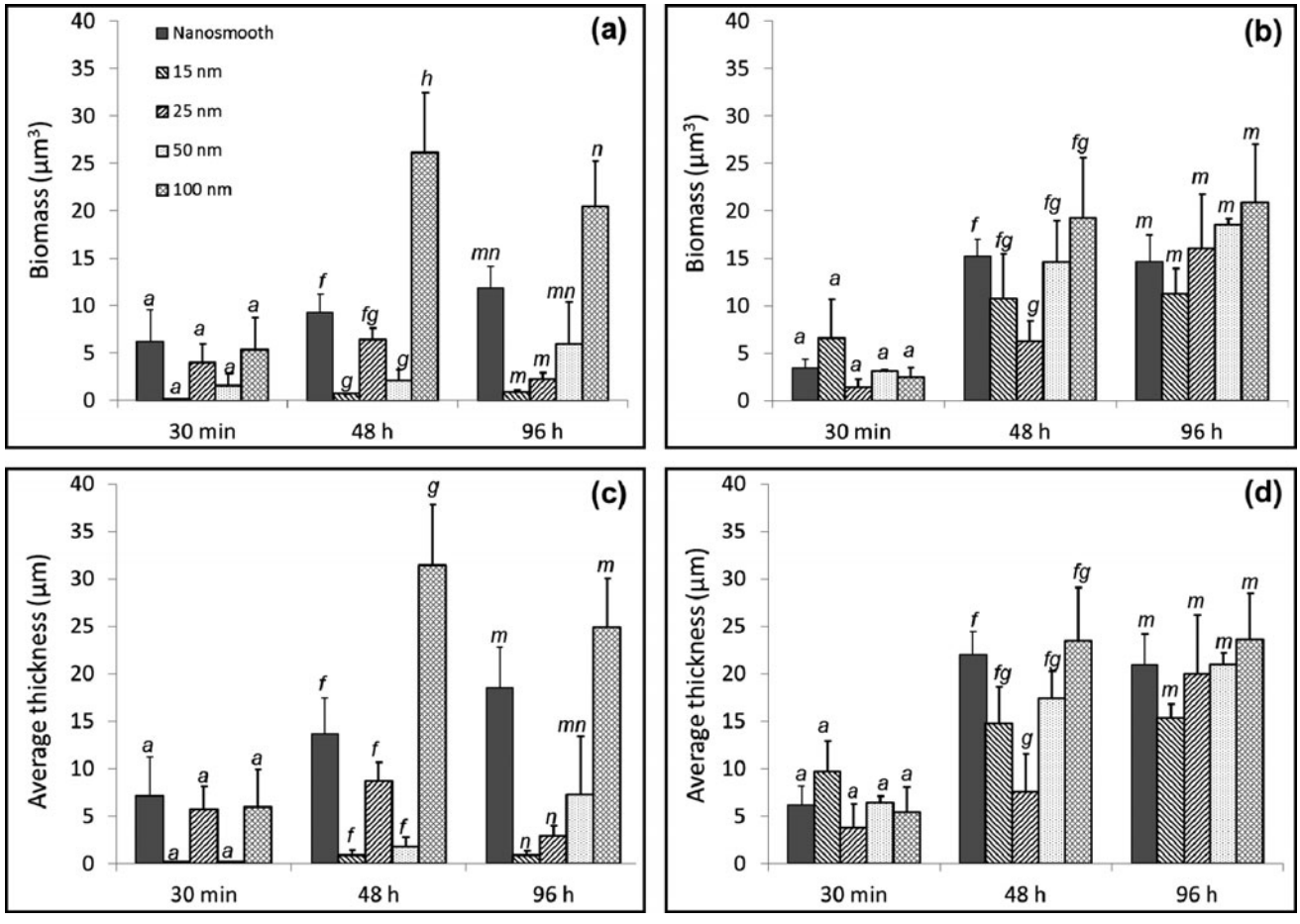

Figure 3. Average values (n = 3) of biomass and thickness of biofilm matrices formed by live *E. coli* ATCC 25922 (a, c) and *L. innocua* (b, d) at 30 min, 48 h and 96 h for all surfaces. For any given time point, values not connected by the same letter are statistically different from each other ($p < 0.05$). Error bars represent the standard error of the means.

about 25 mN m^{-1} (Baier 1980). This relationship was first reported for biofouling in marine applications and has also been found to hold for microorganisms and organic contaminants specific to food processing (Zhao, Liu, Wang, et al. 2005; Zhao, Liu, & Wang 2005; Pereni et al. 2006; Liu et al. 2006; Zhao et al. 2007). However, this theory does not account for the role of the bacterial cells in attachment.

Bacterium–surface interaction is also described by the Derjaguin and Landau, Verwey and Overbeek (DLVO) theory (Marshall et al. 1971), which considers the effect of both surface energy and surface charge on the cell–substratum interactions (Mafu et al. 1991; Carpentier & Cerf 1993; Katsikogianni & Missirlis 2004). According to this theory, the total interaction between a surface and a bacterial cell is the sum of Lifshitz–van der Waals attractive forces, which are dominant in the vicinity of the surface, and electrostatic Coulomb interactions, which become dominant further away from the surface (Hori & Matsumoto 2010). Chen et al. (2014) used atomic force microscopy to derive the long-range Lifshitz–van der Waals adhesion for wild-type *Staphylococcus aureus*, and the measured forces matched those calculated using the DLVO theory, confirming the validity of the DLVO approach. Bacteria and natural surfaces in aqueous solutions are usually negatively charged, which gives rise to a repulsive electrostatic energy (van Loosdrecht et al. 1989). At low ionic strength, when a bacterium approaches a surface it encounters an energy barrier that cannot be overcome solely by motility or Brownian motion; at high ionic strength, this energy barrier vanishes and bacterial cells can easily approach the surface and adhere irreversibly (Bunt et al. 1995; Vigeant & Ford 1997; Otto et al. 1999; Bolster et al. 2001; Hori & Matsumoto 2010). The DLVO theory was later modified into the extended DLVO (XDLVO) theory, which also accounts for hydration forces and hydrophobic forces, summarized as acid–base interaction forces (van Oss 1993). The acid–base interaction forces are dominant in the short-range, but diminish exponentially as separation distance increases (van Oss 1993).

This approach was employed here to estimate the bacteria–surface interaction forces. The total energy needed to bring a bacterium from an infinite distance to a surface is given by (Li & Logan 2004):

$$U_{\mathrm{Total}}^{\mathrm{XDLVO}} = U_{\mathrm{LW}}^{\mathrm{Adj}} + U_{\mathrm{AB}}^{\mathrm{Adj}} + U_{\mathrm{EL}}^{\mathrm{Adj}} \tag{1}$$

The forces associated with these energies are:

$$F_{\mathrm{Total}}^{\mathrm{XDLVO}} = F_{\mathrm{LW}}^{\mathrm{Adj}} + F_{\mathrm{AB}}^{\mathrm{Adj}} + F_{\mathrm{EL}}^{\mathrm{Adj}} \tag{2}$$

where $F_{\mathrm{LW}}^{\mathrm{Adj}}$ represents the Lifshitz–van der Waals attraction forces, $F_{\mathrm{AB}}^{\mathrm{Adj}}$ the acid-base interaction forces and $F_{\mathrm{EL}}^{\mathrm{Adj}}$ the electrostatic repulsive forces.

Since the XDLVO theory is based on smooth surfaces (Bhattacharjee et al. 1996), 'adjusted' (Adj) values of these forces were calculated, taking into consideration the nanoporous structure of the surfaces used in this work. Contributions from the vertical surfaces and the bottoms of the cylindrical pores were also considered.

Moreover, a few simplifying assumptions were made: (i) *E. coli* ATCC 25922 and *L. innocua* cells were assumed to have a spherical shape of equivalent radius of 317 and 492 nm, respectively (Hsu et al. 2013); (ii) surfaces have a fully wetting (Wenzel) behavior (Ran et al. 2008); and (iii) each surface was assumed to be an infinite planar surface in relation to a bacterial cell. Bacterial attachment took place in TSB, approximated as a 1:1 type electrolyte solution of ionic strength $IS = 0.1$ M, at pH 7 and $T = 310$ K. The constants appearing in the expressions for energy (Table 1) and surface zeta potential of pure alumina (Table 2) were taken from the literature. The pore depth and radius, surface porosity of the surface and the dimensions of the bacterial cells were determined from SEM images; zeta potential values of bacterial cells were determined experimentally (Table 2).

The interaction forces exerted on a bacterial cell by a nanostructured substratum was calculated as:

(1) The Lifshitz–van der Waals energy of attraction between the cells and the surfaces, assumed as infinite planar surfaces, was calculated using the retarded Hamaker expression:

$$U_{\mathrm{LW}}(h,d) = \frac{-Ha}{6(h+d)[1+14(h+d)/\lambda]} \tag{3}$$

where H is the Hamaker constant, a is bacterium radius, h is the separation distance between the bacterium and the surface, d is the depth of cylindrical wells and λ is the characteristic wavelength of interaction between the bacteria and the surfaces.

The Hamaker constant is given by:

$$H = -12\pi h_0^2 \Delta G_{\mathrm{LW}} \tag{4}$$

The interaction energy per unit area, ΔG_{LW} between the bacterium and the surface, at the minimum separation distance h_0, is:

$$\Delta G_{\mathrm{LW}} = 2\left(\sqrt{\gamma_{\mathrm{W}}^{\mathrm{LW}}} - \sqrt{\gamma_{\mathrm{S}}^{\mathrm{LW}}}\right)\left(\sqrt{\gamma_{\mathrm{b}}^{\mathrm{LW}}} - \sqrt{\gamma_{\mathrm{W}}^{\mathrm{LW}}}\right) \tag{5}$$

Table 1. Values of constants used for the calculation of bacteria–surface interaction forces.

Symbols	Parameters/constants	Values	Source
λ	Characteristic wavelength of bacteria–surface interaction	100 nm	Gregory (1981)
λ_1	Characteristic decay of acid–base interactions in water	0.6 nm	Bhattacharjee et al. (1996)
ϵ	Permittivity of water	$80 \times 8.8854 \times 10^{-12}$ ($C^2\ J^{-1}\ m^{-1}$)	
h_0	Minimum separation between two bodies	0.158 nm	Bhattacharjee et al. (1996)
k_B	Boltzmann constant	$1.38{\times}10^{23}$ ($J\ K^{-1}$)	
C_e	The elementary charge	$1.602{\times}10^{-19}$ C	
γ	Surface tension of water, glycerol, diiodomethane	(Multiple values)	Li & Logan (2004)

Table 2. Surface properties of bacterial strains and nanosmooth alumina substratum.

	Contact angles (°)			
	Water	Glycerol	Diiodomethane	Zeta potential (mV)
Bacteria				
L. innocua FSL C2-008	46.5±1.2 a	65.9±2.3 a	46.4±1.7 d	−35.3±1.3 b
E. coli ATCC 25922	40.3±1.1 b	70.7±2.1 a	56.9±3.0 c	−29.3±0.4 ab
E. coli K12 WT	22.0±1.6 cd	64.2±3.5 a	67.5±1.2 ab	−24.6±3.5 a
E. coli K12 Δ*flgA*	17.7±1.3 cd	62.1±5.6 a	72.8±0.6 a	−27.3±3.2 ab
E. coli K12 Δ*fimH*	17.3±2.4 d	70.0±0.6 a	64.1±0.8 bc	−33.0±1.2 ab
E. coli K12 Δ*csgA*	21.4±0.2 c	72.1±4.8 a	65.9±1.4 ab	−27.0±1.4 ab
Substratum				
Nanosmooth alumina	67.5±5.0	56.9±1.2	43.7±5.4	−26.2±0.5*

Note: Data are presented as means ± the standard error of the means. Within each column, one-way ANOVA was performed at $\alpha = 0.05$. Within each column, levels not connected by same letter are significantly different ($p < 0.05$).
*Value from Li & Logan (2004).

where superscript 'LW' indicates the non-polar component of surface tension, and subscripts 'w', 'b', and 's' denote water, bacterium, and substratum, respectively.

After adjusting for the presence of nanopores in the surface, Equation 2 becomes:

$$U_{\mathrm{LW}}^{\mathrm{Adj}}(h,d,P) = P * U_{\mathrm{LW}}(h,d) + (1-P) * U_{\mathrm{LW}}(h,0) \tag{6}$$

where P is the porosity of the surface ($P = Area_{\mathrm{pores}}/Area_{\mathrm{total}}$). The adjusted Lifshitz–van der Waals force of attraction is:

$$F_{\mathrm{LW}}^{\mathrm{Adj}} = -\frac{\partial U_{\mathrm{LW}}^{\mathrm{Adj}}}{\partial h} \tag{7}$$

(2) The acid–base interaction between a sphere and infinite planar surface:

$$U_{\mathrm{AB}}(h,d) = 2\pi a \lambda_1 \Delta G_{\mathrm{AB}} e^{\left(\frac{h_0-(h+d)}{\lambda 1}\right)} \tag{8}$$

$$\begin{aligned}\Delta G_{\mathrm{AB}} = {} & 2\sqrt{\gamma_{\mathrm{w}}^{+}}\left(\sqrt{\gamma_{\mathrm{s}}^{-}} + \sqrt{\gamma_{\mathrm{b}}^{-}} - \sqrt{\gamma_{\mathrm{w}}^{-}}\right) \\ & + 2\sqrt{\gamma_{\mathrm{w}}^{-}}\left(\sqrt{\gamma_{\mathrm{s}}^{+}} + \sqrt{\gamma_{\mathrm{b}}^{+}} - \sqrt{\gamma_{\mathrm{w}}^{+}}\right) - 2\left(\sqrt{\gamma_s^{+}\gamma_{\mathrm{b}}^{-}}\right. \\ & \left. + \sqrt{\gamma_b^{+}\gamma_{\mathrm{s}}^{-}}\right)\end{aligned} \tag{9}$$

where superscript '+' indicates the electron acceptor and '–' the electron donor.

The contact angles of three probe liquids on bacterial cells and nanosmooth alumina can be used to determine the surface energy parameters used in Equation 9 by applying the extended Young equation (van Oss 1993):

$$\left(1 + cos\theta_{ij}\right)\gamma_j^{\mathrm{total}} = 2\left(\sqrt{\gamma_i^{\mathrm{LW}}\gamma_j^{\mathrm{LW}}} + \sqrt{\gamma_i^{+}\gamma_j^{-}} + \sqrt{\gamma_i^{-}\gamma_j^{+}}\right) \tag{10}$$

The measured contact angle values used for calculating the polar and non-polar components of the surface energies are provided in Table 2. The contact angles measured on nanosmooth alumina surface are comparable to values found in literature (Li & Logan 2004; Edy et al. 2013). The surface tensions of the three probe solutions, denoted by γ_j, are known constants (van Oss 1993; Brant & Childress 2002).

$U_{\mathrm{AB}}(h,d)$ was modified to account for the contribution of the vertical surface of the cylindrical nanopores. Because the acid–base interactions are short-range interactions, it was considered that only the top rim of the vertical surface of the cylindrical nanopores (within 2 nm from the surface) provides an additional contribution to the acid–base interaction. This portion of the internal surface of the cylindrical pores was approximated as a

ring of N_{hs} hemispheres distributed uniformly along the circumference. The acid–base interaction energy between these spheres (from one cylindrical pore) and the bacterial cell above it $U_{AB}^{ms}(h,d)$, was calculated according to van Oss (1993):

$$U_{AB}^{ms}(h,d) = N_{hs}\frac{1}{2}U_{AB}^{ss}(h,d) = \pi^2\lambda_1\Delta G_{AB}e^{\left(\frac{h_0-h}{\lambda_1}\right)} \quad (11)$$

where $U_{AB}^{ss}(h,d)$ is the acid–base interaction energy between one hemisphere and the bacterial cell. The number of cylindrical nanopores that contribute significantly to the repulsion force exerted on one bacterium is:

$$N_w = P * (R_e/R)^2 \quad (12)$$

where R_e is the radius of the effective circular interaction area (assumed as 60% of the equivalent bacterium radius), P the surface porosity, and R the mean radius of the pores.

The contribution of the N_w cylindrical walls to the total acid–base interaction is:

$$\begin{aligned} U_{AB}^{wall}(h,R,P) &= N_w U_{AB}^{ms}(h,d) \\ &= P * (R_e/R)^2 * \pi^2\lambda_1\Delta G_{AB}e^{\left(\frac{h_0-h}{\lambda_1}\right)} \end{aligned} \quad (13)$$

The total acid–base interaction energy adjusted for the presence of the pores becomes:

$$\begin{aligned} U_{AB}^{Adj}(h,d,R,P) = PU_{AB}(h,d) + (1-P)U_{AB}(h,0) \\ + U_{AB}^{wall}(h,R,P) \end{aligned} \quad (14)$$

Finally, the adjusted acid–base interaction force is:

$$F_{AB}^{Adj} = -\frac{\partial U_{AB}^{Adj}}{\partial h} \quad (15)$$

(3) The electrostatic interaction energy between a bacterium and the surface is:

$$\begin{aligned} U_{EL}(h,d) = \pi\epsilon a\Big\{2\psi_b\psi_s Log\left[\frac{1+e^{-k(h+d)}}{1-e^{-k(h+d)}}\right] \\ + (\psi_b^2+\psi_s^2)Log\left[1-e^{-2k(h+d)}\right]\Big\} \end{aligned} \quad (16)$$

and

$$F_{EL}(h,d) = -\frac{\partial U_{EL}}{\partial h} \quad (17)$$

The total electrostatic force can be treated as the sum of three contributions: (1) from the surface, calculated as $(1-P)*F_{EL}(h,0)$; (2) the bottom of the cylindrical wells, expressed as $P*F_{EL}(h,d)$; and (3) the walls of the cylindrical wells, F_{EL}^{Walls}. F_{EL}^{Walls} is obtained by integrating the electrostatic force element (force exerted on an area element of the bacterium bottom surface by one element of the vertical surface of the pore) over the vertical surface of *one* cylindrical pore. Subsequently, $F_{EL}^{Cen}(h,d)$ was integrated over the circular interaction area (with radius R_i) of the bottom surface of a bacterium cell. Finally the contribution from each pore was multiplied by the number of nanopores within the effective interaction area, N_w, to obtain the electrostatic interaction contributed by the walls:

$$F_{EL}^{Walls}(h,d,R,P) = F_{EL}^{Cen}(h,d)(\pi R_i^2)N_w \quad (18)$$

where $F_{EL}^{Cen}(h,d)$ is the electrostatic force per unit bacterium surface area exerted by a cylindrical pore of depth d and R_i is the radius of the circular interaction area on the bottom surface of a bacterium cell where the electrostatic interaction is significant.

To determine $F_{EL}^{Cen}(h,d)$, the surface charge density of the bacterial cell and the substratum were calculated using the Grahame equation (Grahame 1953):

$$\begin{aligned} \sigma(\psi_i,M_1,M_2) = \sqrt{8\epsilon k_B T}\mathrm{Sinh}[C_e\psi_i/2k_BT][M_1+M_2(2 \\ + e^{-C_e\psi_i/k_BT})]^{1/2} \end{aligned} \quad (19)$$

where M_1 and M_2 are the bulk concentration of monovalent cations and divalent cations (estimated to be 0.1 M and 0 for TSB, respectively); C_e is the elementary charge; and ψ_i is the surface potential of the bacteria or the substrate. Surface potentials were assumed to be the same as the corresponding zeta potentials (Li & Logan, 2004).

The total electrostatic interaction force adjusted for the presence of the pores becomes:

$$F_{EL}^{Adj} = P * F_{EL}(h,d) + (1-P) * F_{EL}(h,0) + F_{EL}^{Walls} \quad (20)$$

Figure 4a, b shows examples of interaction forces between the cells and the 15 nm surface as a function of the separation distance from the surface, for *E. coli* ATCC 25922 and *L. innocua*, respectively. Figure 5a, b shows the total force, F_{Total}^{XDLVO}, calculated for each surface as a function of the separation distance. By convention, forces pointing towards the surface (attractive forces) are negative, while forces pointing away from the surface (repulsion forces) are positive (Li & Logan 2004).

In close proximity of the alumina surface, within fractions of a nanometer, the bacterium–surface interaction force for both *E. coli* and *L. innocua* is attractive for all surfaces, primarily due to the short range attractive Lifshitz–van der Waals forces, which are dominant at this length scale. The acid–base interaction force, dominant for a separation distance of several nanometers away from the surface, is strongly repulsive for *E. coli*

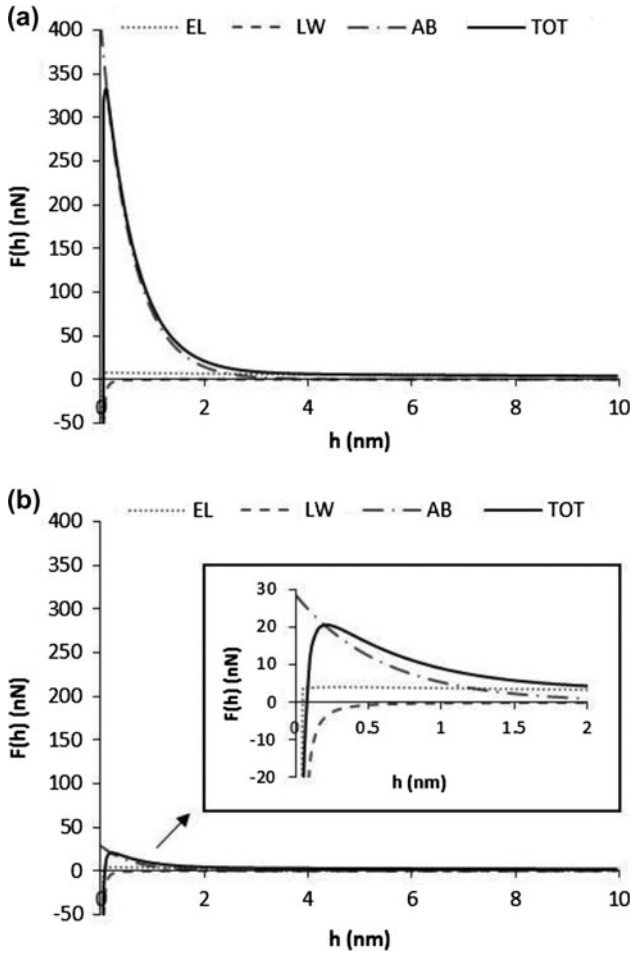

Figure 4. Interaction forces between bacterial cells and the 15 nm alumina surface as a function of separation distance between cells and the surface for (a) *E. coli* ATCC 25922 and (b) *L. innocua* (the inset shows a magnified plot). EL: electrostatic force; LW: Lifshitz–van der Waals forces; AB: acid–base interaction force; TOT: total interaction force.

(Figure 4a) at all separation distances from the surface, but mildly so for *L. innocua* (Figure 4b). For both microorganisms, the dominant contribution to $F_{\text{Total}}^{\text{XDLVO}}$ for a separation distance beyond a few nanometers comes from the repulsive electrostatic force, though the maximum of this electrostatic force is only about 1/40 of the maximum of the acid–base interaction force for *E. coli* ATCC 25922, or 1/5 for *L. innocua* on a 15 nm surface. These observations are in agreement with the relative magnitude of forces reported in previous studies (van Oss 1993; Brant & Childress 2002). As a result of the tremendous increase in the bacteria–surface interaction area contributed by the cylindrical walls, the acid–base interaction force, and consequently, the total repelling force F_{Total}^{XDLVO} increased substantially as the density of vertical pores per unit surface area increased, which was the case for the 15 and 25 nm pore surfaces.

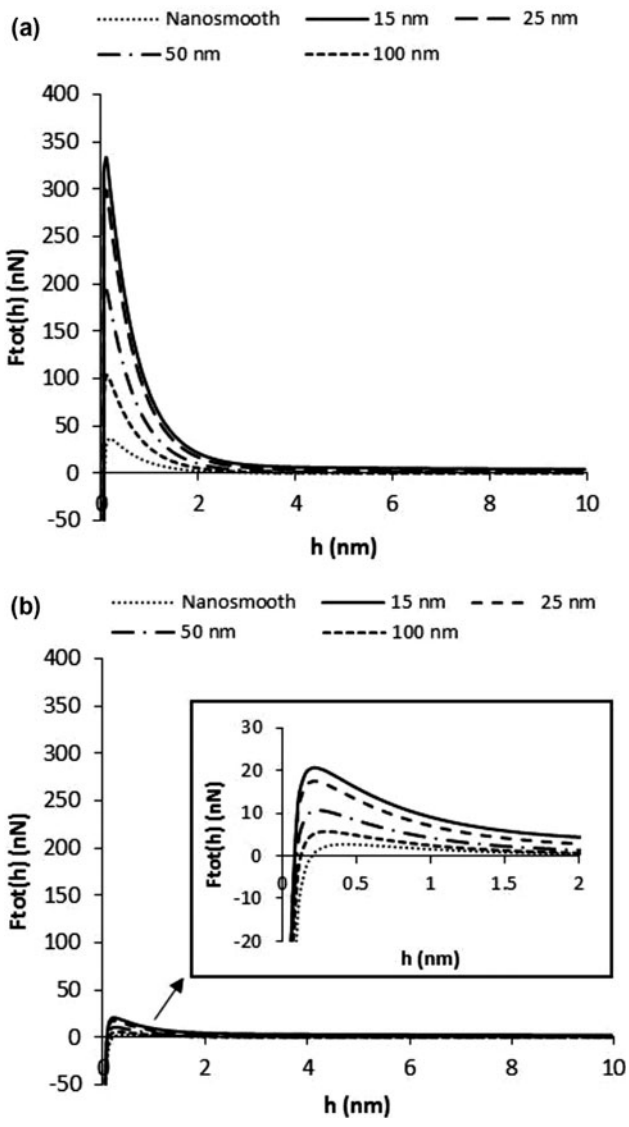

Figure 5. Total force exerted by the surfaces on the bacteria cells as a function of distance from the substratum surface for: (a) *E. coli* ATCC 25922 and (b) *L. innocua* (the inset represents a magnified plot). D: pore diameter.

The maximum total repulsive force (F_{max}) correlated very well with the number of cells attached to the surface, as shown in Figure 6. The number of cells was estimated by dividing the biomass volume for each strain–surface pair by the volume of an individual cell of that strain. The average cell volumes were calculated based on the cell size data (Hsu et al. 2013), and were 0.50 μm^3 $cell^{-1}$ for *E. coli* ATCC 25922 and 0.13 μm^3 $cell^{-1}$ for *L. innocua.*

For both microorganisms, the 15 nm pore surfaces exerted the largest peak repulsive force (F_{max}) followed by the 25 nm pore surfaces, with the 50 nm pore surface, 100 nm pore surface and the control exerting comparable,

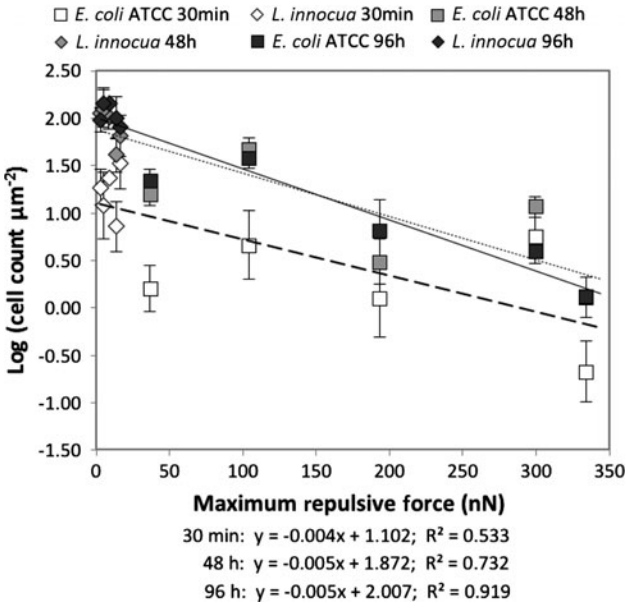

Figure 6. Correlation between cell count per unit area and the peak value of the total interaction (repulsive) force between bacteria and the surfaces (calculated according to Equation 2) at 30 min, 48 h, and 96 h. Error bars represent the standard error of the means (n = 3).

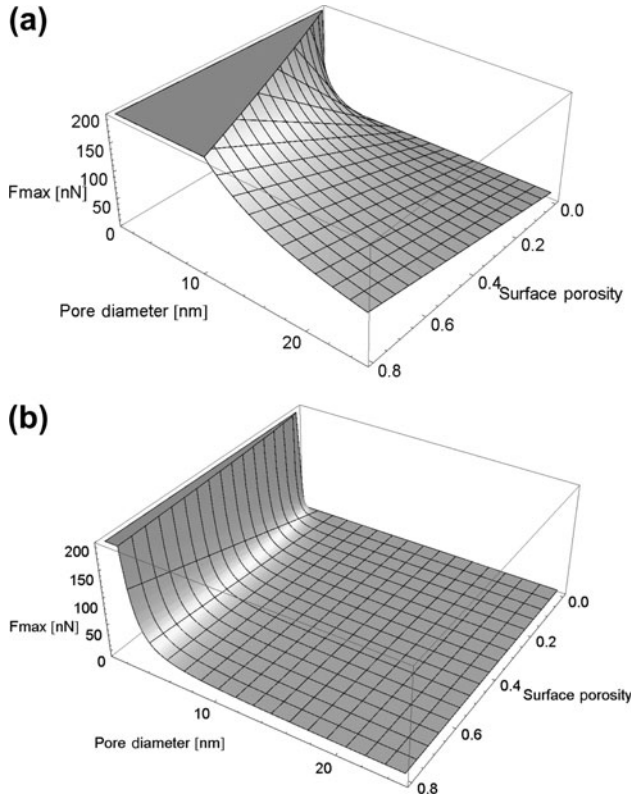

Figure 7. Theoretical predictions of the change in maximum repulsion force as a function of pore diameter and surface porosity, at fixed pore depth (1 µm) for (a) *E. coli* and (b) *L. innocua.*

and relatively low, F_{max}. Figure 6 shows a linear decrease in cell counts (expressed as log CFU per unit area) as a function of F_{max} for both organisms and all time points. The F_{max} exerted on *E. coli* is stronger than that on *L. innocua*, hence the biomass accumulation is less.

The R^2 value of the regression lines was the weakest at 30 min, and the highest at 96 h. This can be explained at least in part by the improvement in the signal-to-noise ratio of the data from 30 min (the lowest number of cells attached) to 96 h (the highest number of cells). This correlation is very important, as it relates the bacterium–surface interaction forces with attachment and biofilm formation on the alumina surfaces, for both microorganisms used in this study. This correlation offers a significant insight into the mechanisms that control bacterial attachment, and may be used as a predictive tool for the development of antifouling and antimicrobial surfaces.

Theoretical calculations have been performed to better understand the effect of various surface topological characteristics on the total interaction force. Figure 7 summarizes these calculations by showing the effect of pore diameter and surface porosity on F_{max} for both challenge organisms. Pore diameter has a tremendous effect on the repulsive force, particularly at pore diameters below 20 nm, with repulsive forces increasing exponentially as pore diameter decreases, at a fixed surface porosity. An increase in porosity at a fixed diameter induces a linear increase in the value of the repulsive force, while pore depth does not seem to have a significant effect above several tens of nanometers. This is well below the depth of pores of anodized surfaces, which are several micrometers deep. Hence, controlling the pore diameter, porosity and number of pores per unit area is key in tuning the total repulsive force and preventing initial attachment. It must also be noted that F_{max} exerted on *E. coli* ATCC 25922 varies more substantially in response to changes in porosity and pore diameter as compared to *L. innocua*, illustrating the significant role of cell surface properties in the attachment process. This suggests that theoretical calculations of the physicochemical interaction between each specific bacterium–surface pair are essential to making accurate predictions of bacterial attachment.

Effect of anodized surfaces on bacterial cells

Although physico-chemical interactions between the substratum and the bacterial cells seem to play a major role in attachment, attachment is likely also due to biological changes experienced by the cells in response to surface topography. Surface topography has been shown to induce morphological, transcriptomic and proteomic

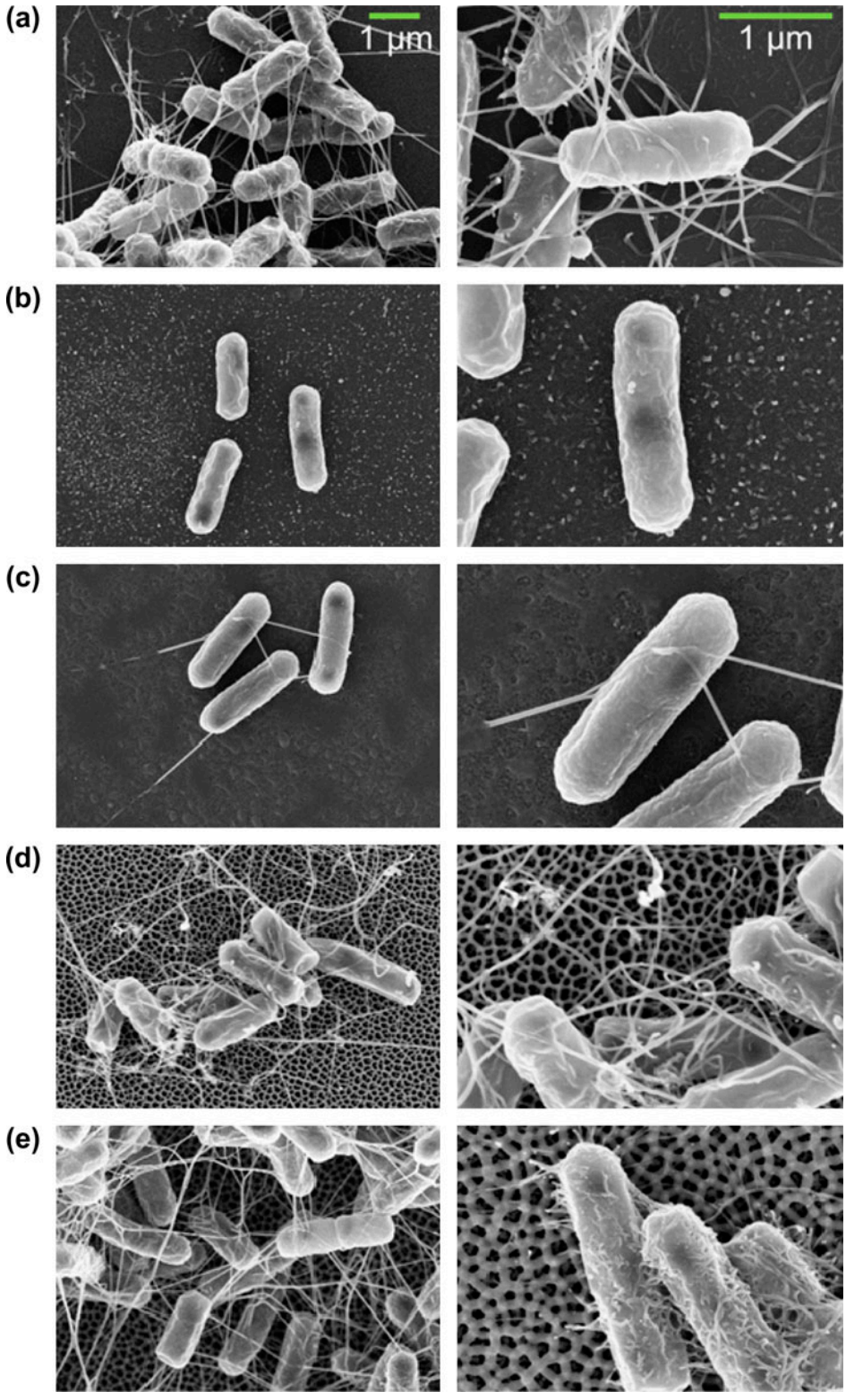

Figure 8. SEM images of *E. coli* cells attached to (a) nanosmooth, (b) 15 nm, (c) 25 nm, (d) 50 nm and (e) 100 nm pore surfaces. Lower magnification images (left) show microbial communities and higher magnification images (right) show details of bacterial structures that physically interact with the surfaces. These images are representative of at least 10 observed fields.

shifts in bacteria (Schilling & Bowen 1992; Prigent-Combaret et al. 2000; Whitchurch et al. 2002; Harmsen et al. 2010; Hsu et al. 2013). A comprehensive understanding of how nanoscale topography affects the expression of biomolecular entities that play a role in attachment is not available at present. An aspect somewhat well understood is the surface effect on cellular adhesins. Rizzello et al. (2011) reported that *E. coli* cells grown on nanostructured surfaces lost the expression of fimbriae, which are considered critical virulence factors required for initial attachment (Naves et al. 2008). *E. coli* is known for its ability to develop cellular appendages, such as pili and flagella, which have a strong role in the later stages of microbial attachment and biofilm formation (Hori & Matsumoto 2010). Bacteria may use these small diameter cellular appendages to penetrate the energy barrier produced by the repulsive physico-chemical forces, facilitating cell attachment to an otherwise repelling surface.

The SEM examination of surfaces with attached cells show a striking difference between the type and number of appendages expressed by *E. coli* on the various surfaces (Figure 8), which is consistent with earlier observations (Hsu et al. 2013). The appendages observed in this study resemble closely those observed by Prigent-Combaret et al. (2000) for curli-producing *E. coli* strains. The structure of these appendages was distinct from that of extracellular polymeric substances (EPS) produced by *E. coli* (Figure S1). The *E. coli* cells imaged on the nanosmooth control (Figure 8a) and the larger pore anodic surfaces (Figure 8d, e) appear clustered in a complex architecture, and feature a large number of long, intertwined appendages. In contrast, the *E. coli* cells on the 15 and 25 nm surfaces appear as isolated cells and feature only few, relatively short appendages (Figure 8b, c). From SEM images, the diameter of the appendages expressed by the *E. coli* cells was estimated as 30–60 nm. For surfaces with pore diameters above this size, the appendages can easily penetrate inside the pores, which will help anchor the cells onto the surface. This was clearly observed for the 50 and 100 nm surfaces, for which appendages were seen to penetrate inside the pores (Figure 8d, e). No cellular appendages were observed for *L. innocua* under the tested conditions.

Role of bacterial appendages in the attachment process

An attachment assay was conducted using *E. coli* K12 appendage-deficient mutants, since there were no appendage-deficient mutants available for *E. coli* ATCC 25922 used in the rest of the study.

The flagellum-deficient mutant (*ΔflgA*) showed lower attachment to both 15 and 100 nm surfaces compared with the wild type strain (Figure 9), suggesting that flagella have a significant role in attachment to the anodized

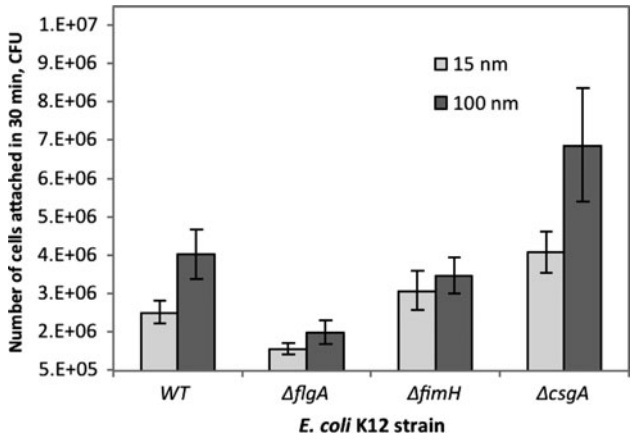

Figure 9. Attachment at 30 min by *E. coli* K12 wild type, flagella-, fimbria- and curli-deficient mutants on 15 and 100 nm surfaces. Error bars represent the standard error of the means.

surfaces. The difference in attachment between WT and the fimbriae-deficient mutant (*ΔfimH*) was negligible on either surface type, implying that fimbria may play a minor role in the initial attachment. Interestingly, the curli-deficient mutant (*ΔcsgA*) attached to both surfaces at the highest level among all *E. coli* K12 strains. Previous findings revealed that the loss of *csgA* expression could result in reduction of biofilm formation (Vidal et al. 1998; Dorel et al. 1999) and that curli have a significant role in the structural integrity of mature biofilm matrices (Serra et al. 2013). The discrepancy could be due to the fact that short-term attachment rather than biofilm formation was assessed in this study. Beaussart et al. (2014) quantified the forces guiding the adhesion of *Pseudomonas aeruginosa* to surfaces and showed that type IV pili strongly bind to hydrophobic biotic and abiotic surfaces in a time-dependent manner, while flagella and the pili-associated adhesin PilY1 played no direct role, further substantiating the complexity of bacterial attachment and the need for further work in this area.

Nonetheless, in the current study, attachment to the 100 nm surface was higher than on the 15 nm surface, consistent with the observations from the attachment study with *E. coli* ATCC 25922 and *L. innocua*. However, differences in attachment were statistically significant only for the wild type and the curli-deficient *E. coli* K12 strains.

Measurements of water contact angles and zeta potential for the *E. coli* K12 strains (Table 2) indicated that the genetic modifications did not result in any significant change in cell hydrophobicity or electrical charge. Therefore, the differences in attachment observed between the WT and appendage-deficient mutants were most likely biological in nature, highlighting the role of surface adhesins in attachment. It is possible that the strength of attachment by the different strains to the two

surfaces was different, with a potentially stronger attachment to the 100 nm surfaces, but this hypothesis will have to be tested in future experiments.

Conclusions

This study reveals the direct effect of the pore diameter of anodic nanoporous alumina on the attachment behavior and biofilm formation by Gram-positive and Gram-negative bacterial strains. Nanoporous surfaces with pore diameters of 15 and 25 nm and relatively large surface porosity were able to effectively minimize attachment by *E. coli* spp. and *Listeria* spp., and possibly by other microorganisms. The physico-chemical properties of the anodized surfaces, which are directly affected by pore diameter and surface porosity, and the cell surface, as well as appendages expressed by bacterial cells were shown to play an important role in attachment.

These findings can be used to design and fabricate affordable antifouling surfaces for food and water processing, as well as dentistry or biomedical applications, with substantial public health and economic benefits. Engineering nanoporous anodized surfaces with antifouling properties could translate into virtually immediate applications, since technology transfer for using anodic surfaces in numerous applications can be very rapid.

Acknowledgements

This project was supported by USDA-NIFA (Project 65210–20024–11). This work made use of the Cornell Center for Materials Research (CCMR) Shared Facilities, supported through the NSF MRSEC program (DMR-1120296), Cornell University Biotechnology Resource Center (BRC) Imaging Facility, with support from NIH 1S10RR025502-01, and the Cornell Nanobiotechnology Center (NBTC), supported by NSF (Agreement No. ECS-9876771). The authors are grateful for the assistance from Penny D. Burke (NBTC), Teresa Porri (NBTC), John A. Hunt (CCMR), Malcolm Thomas (CCMR), John L. Grazul (CCMR), and Carol J. Bayles (BRC).

References

Arnold JW, Bailey GW. 2000. Surface finishes on stainless steel reduce bacterial attachment and early biofilm formation: scanning electron and atomic force microscopy study. Poult Sci. 79:1839–1845.

Baba T, Ara T, Hasegawa M, Takai Y, Okumura Y, Baba M, Datsenko KA, Tomita M, Wanner BL, Mori H. 2006. Construction of *Escherichia coli* K-12 in-frame, single-gene knockout mutants: the Keio collection. Mol Syst Biol. 2 (2006):0008.

Baier RE. 1980. Substrata influences on the adhesion of microorganisms and their resultant new surface properties. In: Bitton G, Marshall KC, editors. Adsorpt micro-organisms to surfaces. New York: John Wiley & Sons; p. 59–104.

Beaussart A, Baker AE, Kuchma SL, El-Kirat-Chatel S, O'Toole GA, Dufrêne YF. 2014. Nanoscale adhesion forces of *Pseudomonas aeruginosa* Type IV Pili. ACS Nano. 8:10723–10733.

Bhattacharjee S, Sharma A, Bhattacharya PK. 1996. Estimation and influence of long range solute. membrane interactions in ultrafiltration. Ind Eng Chem Res. 35:3108–3121.

Bolster CH, Mills AL, Hornberger GM, Herman JS. 2001. Effect of surface coatings, grain size, and ionic strength on the maximum attainable coverage of bacteria on sand surfaces. J Contam Hydrol. 50:287–305.

Boulangé-Petermann L, Rault J, Bellon-Fontaine M. 1997. Adhesion of *Streptococcus thermophilus* to stainless steel with different surface topography and roughness. Biofouling. 11:201–216.

Brant J a., Childress AE. 2002. Membrane–colloid interactions: comparison of extended DLVO predictions with AFM force measurements. Environ Eng Sci. 19:413–427.

Bryers JD. 2009. Medical biofilms. Biotech Bioeng. 100:1–18.

Bunt CR, Jones DS, Tucker IG. 1995. The effects of pH, ionic strength and polyvalent ions on the cell surface hydrophobicity of *Escherichia coli* evaluated by the BATH and HIC methods. Int J Pharm. 113:257–261.

Busscher HJ, Weerkamp AH, van der Mei HC, van Pelt AW, de Jong HP, Arends J. 1984. Measurement of the surface free energy of bacterial cell surfaces and its relevance for adhesion. Appl Environ Microbiol. 48:980–983.

Carpentier B, Cerf O. 1993. Biofilms and their consequences, with particular reference to hygiene in the food industry. J Appl Microbiol. 75:499–511.

Chen Y, Harapanahalli AK, Busscher HJ, Norde W, van der Mei HK. 2014. Nanoscale cell wall deformation impacts long-range bacterial adhesion forces on surfaces. Appl Environ Microbiol. 80(2):637–643.

Díaz C, Schilardi PL, Salvarezza RC, de Mele MFL. 2007. Nano/microscale order affects the early stages of biofilm formation on metal surfaces. Langmuir. 23:11206–11210.

Dorel C, Vidal O, Prigent-Combaret C, Vallet I, Lejeune P. 1999. Involvement of the Cpx signal transduction pathway of *E. coli* in biofilm formation. FEMS Microbiol Lett. 178:169–175.

Edy R, Huang X, Guo Y, Zhang J, Shi J. 2013. Influence of argon plasma on the deposition of Al_2O_3 film onto the PET surfaces by atomic layer deposition. Nanoscale Res Lett. 8:79.

Feng G, Klein MI, Gregoire S, Singh AP, Vorsa N, Koo H. 2013. The specific degree-of-polymerization of A-type proanthocyanidin oligomers impacts *Streptococcus mutans* glucan-mediated adhesion and transcriptome responses within biofilms. Biofouling. 29:629–640.

Friedlander RS, Vlamakis H, Kim P, Khan M, Kolter R, Aizenberg J. 2013. Bacterial flagella explore microscale hummocks and hollows to increase adhesion. Proc Natl Acad Sci USA. 110:5624–5629.

Grahame DC. 1953. Diffuse double layer theory for electrolytes of unsymmetrical valence types. J Chem Phys. 21:1054–1060.

Gregory J. 1981. Approximate expression for retarded van dar Waals interaction. J Colloid Interface Sci. 83:138–145.

Harmsen M, Lappann M, Knøchel S, Molin S. 2010. Role of extracellular DNA during biofilm formation by *Listeria monocytogenes*. Appl Environ Microbiol. 76:2271–2279.

Heydorn A, Nielsen a T, Hentzer M, Sternberg C, Givskov M, Ersbøll BK, Molin S. 2000. Quantification of biofilm structures by the novel computer program COMSTAT. Microbiology. 146:2395–2407.

Hori K, Matsumoto S. 2010. Bacterial adhesion: from mechanism to control. Biochem Eng J. 48:424–434.

Hsu L, Fang J, Borca-Tasciuc D, Worobo R, Moraru CI. 2013. The effect of micro- and nanoscale topography on the adhesion of bacterial cells to solid surfaces. Appl Environ Microbiol. 79:2703–2712.

Jessensky O, Müller F, Gösele U. 1998. Self-organized formation of hexagonal pore arrays in anodic alumina. Appl Phys Lett. 72:1173–1175.

Katsikogianni M, Missirlis YF. 2004. Concise review of mechanisms of bacterial adhesion to biomaterials and of techniques used in estimating bacteria-material interactions. Eur Cell Mater. 8:37–57.

Kim JK, Harrison MA. 2009. Surrogate selection for *Escherichia coli* O157:H7 based on cryotolerance and attachment to romaine lettuce. J Food Prot. 72:1385–1391.

Lemon KP, Higgins DE, Kolter R. 2007. Flagellar motility is critical for *Listeria monocytogenes* biofilm formation. J Bacteriol. 189:4418–4424.

Li B, Logan BE. 2004. Bacterial adhesion to glass and metal-oxide surfaces. Colloids Surf B Biointerfaces. 36:81–90.

Liu W, Fryer PJ, Zhang Z, Zhao Q, Liu Y. 2006. Identification of cohesive and adhesive effects in the cleaning of food fouling deposits. Innov Food Sci Emerg Tech. 7:263–269.

Mafu AA, Roy D, Goulet J, Savoie L. 1991. Characterization of physicochemical forces involved in adhesion of *Listeria monocytogenes* to surfaces. Appl Environ Microbiol. 57:1969–1973.

Marshall KC, Stout R, Mitchell R. 1971. Mechanism of the initial events in the sorption of marine bacteria to surfaces. J Gen Microbiol. 68:337–348.

Masuda H, Yada K, Osaka A. 1998. Self-ordering of cell configuration of anodic porous alumina with large-size pores in phosphoric acid solution. Jpn J Appl Phys. 37:L1340–L1342.

Mauclaire L, Brombacher E, Bünger JD, Zinn M. 2010. Factors controlling bacterial attachment and biofilm formation on medium-chain-length polyhydroxyalkanoates (mcl-PHAs). Colloids Surf B Biointerfaces. 76:104–111.

Medilanski E, Kaufmann K, Wick LY, Wanner O, Harms H. 2002. Influence of the surface topography of stainless steel on bacterial adhesion. Biofouling. 18:193–203.

Naves P, del Prado G, Huelves L, Gracia M, Ruiz V, Blanco J, Dahbi G, Blanco M, Ponte MDC, Soriano F. 2008. Correlation between virulence factors and *in vitro* biofilm formation by *Escherichia coli* strains. Microb Pathog. 45:86–91.

Niba ETE, Naka Y, Nagase M, Mori H, Kitakawa M. 2007. A genome-wide approach to identify the genes involved in biofilm formation in *E. coli*. DNA Res. 14:237–246.

Oliveira R, Azeredo J, Teixeira P, Fonseca AP. 2001. The role of hydrophobicity in bacterial adhesion. Biofilm community Interact chance or necessity? BioLine for the Biofilm Club. 11–22.

Otto K, Elwing H, Hermansson M. 1999. Effect of ionic strength on initial interactions of *Escherichia coli* with surfaces, studied on-line by a novel quartz crystal microbalance technique. J Bacteriol. 181:5210–5218.

Park MR, Banks MK, Applegate B, Webster TJ. 2008. Influence of nanophase titania topography on bacterial attachment and metabolism. Int J Nanomedicine. 3:497–504.

Pereni CI, Zhao Q, Liu Y, Abel E. 2006. Surface free energy effect on bacterial retention. Colloids Surf B Biointerfaces. 48:143–147.

Prigent-Combaret C, Prensier G, Le Thi TT, Vidal O, Lejeune P, Dorel C. 2000. Developmental pathway for biofilm formation in curli-producing *Escherichia coli* strains: role of flagella, curli and colanic acid. Environ Microbiol. 2:450–464.

Puckett SD, Taylor E, Raimondo T, Webster TJ. 2010. The relationship between the nanostructure of titanium surfaces and bacterial attachment. Biomaterials. 31:706–713.

Ran C, Ding G, Liu W, Deng Y, Hou W. 2008. Wetting on nanoporous alumina surface: transition between Wenzel and Cassie states controlled by surface structure. Langmuir. 24:9952–9955.

Rijnaarts HHM, Norde W, Lyklema J, Zehnder AJB. 1999. DLVO and steric contributions to bacterial deposition in media of different ionic strengths. Colloids Surf B Biointerfaces. 14:179–195.

Rizzello L, Sorce B, Sabella S, Vecchio G, Galeone A, Brunetti V, Cingolani R, Pompa PP. 2011. Impact of nanoscale topography on genomics and proteomics of adherent bacteria. ACS Nano. 5:1865–1876.

Saini JK, Marsden JL, Fung DYC, Crozier-Dodson BA. 2012. Evaluation of potential for translocation of *Listeria monocytogenes* from floor drains to food contact surfaces in the surrounding environment using *Listeria innocua* as a surrogate. Adv Microbiol. 02:565–570.

Scharff RL. 2012. Economic burden from health losses due to foodborne illness in the United States. J Food Prot. 75:123–131.

Schilling KM, Bowen WH. 1992. Glucans synthesized *in situ* in experimental salivary pellicle function as specific binding sites for *Streptococcus mutans*. Infect Immun. 60:284–295.

Serra DO, Richter AM, Klauck G, Mika F, Hengge R. 2013. Microanatomy at cellular resolution and spatial order of physiological differentiation in a bacterial biofilm. MBio. 4:e00103–13.

Singh AV, Vyas V, Patil R, Sharma V, Scopelliti PE, Bongiorno G, Podestà A, Lenardi C, Gade WN, Milani P. 2011. Quantitative characterization of the influence of the nanoscale morphology of nanostructured surfaces on bacterial adhesion and biofilm formation. PLoS One. 6:e25029.

Taylor P, Jorge P, Lourenço A, Pereira MO. 2012. New trends in peptide-based anti-biofilm strategies: a review of recent achievements and bioinformatic approaches. Biofouling. 28:1033–1061.

Thomas P, Benaben P. 2007. Preparation of highly ordered nanoporous alumina by two step anodising: process and industrial applications. Trans Inst Met Finish. 85:212–216.

Tide C, Harkin SR, Geesey GG, Bremer PJ, Scholz W. 1999. The influence of welding procedures on bacterial colonization of stainless steel weldments. J Food Eng. 42:85–96.

van Loosdrecht MCM, Lyklema J, Norde W, Zehnder AJB. 1989. Bacterial adhesion: a physicochemical approach. Microb Ecol. 17:1–15.

van Oss CJ. 1993. Acid-base interfacial interactions in aqueous media. Colloids Surf A Physicochem Eng Asp. 78:1–49.

Verran J, Boyd RD. 2001. The relationship between substratum surface roughness and microbiological and organic soiling: a review. Biofouling. 17:59–71.

Verran J, Packer A, Kelly P, Whitehead KA. 2010. The retention of bacteria on hygienic surfaces presenting scratches of microbial dimensions. Lett Appl Microbiol. 50:258–263.

Vidal O, Longin R, Prigent-combaret C, Hooreman M, Lejeune P. 1998. Isolation of an *Escherichia coli* K-12 mutant strain able to form biofilms on inert surfaces: involvement of a new ompR allele that increases curli expression. J Bacteriol. 180:2442–2449.

Vigeant MA, Ford RM. 1997. Interactions between motile *Escherichia coli* and glass in media with various ionic strengths, as observed with a three-dimensional-tracking microscope. Appl Environ Microbiol. 63:3474–3479.

Whitchurch CB, Tolker-Nielsen T, Ragas PC, Mattick JS. 2002. Extracellular DNA required for bacterial biofilm formation. Science. 295:1487.

Whitehead K, a, Colligon J, Verran J. 2005. Retention of microbial cells in substratum surface features of micrometer and sub-micrometer dimensions. Colloids Surf B Biointerfaces. 41:129–138.

Xu L-C, Siedlecki CA. 2012. Submicron-textured biomaterial surface reduces staphylococcal bacterial adhesion and biofilm formation. Acta Biomater. 8:72–81.

Zhao Q, Liu Y, Wang C, Wang S, Müller-Steinhagen H. 2005. Effect of surface free energy on the adhesion of biofouling and crystalline fouling. Chem Eng Sci. 60:4858–4865.

Zhao Q, Liu Y, Wang C. 2005. Development and evaluation of electroless Ag-PTFE composite coatings with antimicrobial and anti-corrosion properties. Appl Phys Lett. 252:1620–1627.

Zhao Q, Wang C, Liu Y, Wang S. 2007. Bacterial adhesion on the metal-polymer composite coatings. Int J Adhes Adhes. 27:85–91.